Magnetic Transitions in the Cyano-Bridged Bimetallic Ferromagnet $Mn_2(H_2O)_5Mo(CN)_7 \cdot 4.75H_2O$ (β Phase)

Joulia Larionova,[†] Olivier Kahn,*[,†] Stéphane Golhen,[‡] Lahcène Ouahab,[‡] and Rodolphe Clérac[†,§]

Laboratoire des Sciences Moléculaires, Institut de Chimie de la Matière Condensée de Bordeaux, UPR CNRS No. 9048, 33608 Pessac, France, Laboratoire de Chimie du Solide et Inorganique Moléculaire, UMR CNRS No. 6511, Université de Rennes 1, 35042 Rennes, France, and Centre de Recherche Paul Pascal, UPR CNRS No. 8641, 33600 Pessac, France

Received October 29, 1998

Slow diffusion of two aqueous solutions containing $K_4[Mo(CN)_7]\cdot 2H_2O$ and $[Mn(H_2O)_6](NO_3)_2$, respectively, has afforded two kinds of single crystals whose formulas are $Mn_2(H_2O)_5Mo(CN)_7]\cdot 4H_2O$ (α phase) and $Mn_2(H_2O)_5Mo(CN)_7]\cdot 4.75H_2O$ (β phase). This paper is devoted to the latter compound. It crystallizes in the monoclinic system, space group $P2_1/c$, $a = 7.885(3)$ Å, $b = 10.406(7)$ Å, $c = 25.233(11)$ Å, $\beta = 98.11(2)°$, $Z = 4$. The Mo site is surrounded by seven −C−N−Mn linkages in a distorted pentagonal bipyramid fashion. There are two distorted octahedral Mn sites, one with four and the other with three −N−C−Mo linkages. The structure is three-dimensional. It consists of bent ladders made of edge-sharing $(MoCNMnNC)_2$ lozenge motifs running along the *a* direction. These ladders are linked further along the *a* and *c* directions. The *a*, *b*, and *c** axes were determined to be the magnetic axes. Both temperature and field dependence of the magnetization have been measured along the magnetic axes. The angular dependence of the magnetization in the *ab* plane as a function of the external field has also been measured. Single crystal magnetic measurements revealed that the compound orders ferromagnetically at $T_c = 51$ K, without a hysteresis effect. They have also shown that the compound has a complex magnetic phase diagram when the field is applied along the *a* direction, with several ferromagnetically ordered domains and a spin reorientation domain. The boundaries between these domains have been determined. These results have been compared to those obtained with $Mn_2(H_2O)_5Mo(CN)_7]\cdot 4H_2O$ (α phase).

Introduction

Recently, we initiated a new project of research dealing with the design and the physical studies of cyano-bridged bimetallic magnetic materials obtained from the $[Mo(CN)_7]^{4-}$ precursor.[1−3] This project was motivated by the idea that these compounds could exhibit magnetic properties very different from those reported for the Prusssian-Blue phases.[4−23] In particular, the use of the heptacoordinated $[Mo(CN)_7]^{4-}$ precursor prevented us from obtaining compounds with the face-centered cubic structure of the Prussian-Blue phases. Therefore, our novel cyano-bridged compounds were anticipated to exhibit interesting anisotropy properties. This expectation was strengthened by the strong local anisotropy of $[Mo(CN)_7]^{4-}$. In an ideal pentagonal bipyramid geometry with D_{5h} symmetry, $[Mo(CN)_7]^{4-}$ has an $^2E''_1$ ground state.[24] This state is split into two Kramers doublets by spin−orbit coupling. The **g** tensor associated with the lowest Kramers doublet has been reported to be very anisotropic with $g_x = g_y = 1.77$ and $g_z = 3.89$.[25] Of course, for a thorough investigation

* Corresponding author.
† ICMCB.
‡ LCSIM.
§ CRPP.

(1) Larionova, J.; Sanchiz, J.; Golhen, S.; Ouahab, L.; Kahn, O. *J. Chem. Soc., Chem. Commun.* **1998**, 953.
(2) Larionova, J.; Clerac, R.; Sanchiz, J.; Kahn, O.; Golhen, S.; Ouahab, L. *J. Am. Chem. Soc.* **1998**, *120*, 13088.
(3) Larionova, J.; Kahn, O.; Golhen, S.; Ouahab, L.; Clerac, R. *J. Am. Chem. Soc.* **1999**, *121*, 3349.
(4) Bozorth, R. M.; Williams, H. J.; Walsh, D. E. *Phys. Rev.* **1956**, *103*, 572.
(5) Holden, A. N.; Matthias, B. T.; Anderson, P. W.; Lewis, H. W. *Phys. Rev.* **1956**, *102*, 1463.
(6) Herren, F.; Fischer, P.; Ludi, A.; Hälg, W. *Inorg. Chem.* **1980**, *19*, 9, 956.
(7) Ludi, A.; Güdel, H. U. *Struct. Bonding (Berlin)* **1973**, *14*, 1.
(8) Klenze, R.; Kanellakopoulos, B.; Trageser, G.; Eysel, H. *J. Chem. Phys.* **1980**, *72*, 5819.
(9) Griebler, W. D.; Babel, D. Z. *Z. Naturforsch. B* **1982**, *37*, 832.
(10) Babel, D. *Comments Inorg. Chem.* **1986**, *5*, 285.
(11) Babel, D.; Kurtz, W. In *Solid State Chemistry 1982*; Metselaar, R. Heijligers, H. J. M., Schoonman, J., Eds.; Elsevier: Amsterdam, 1983.
(12) Kurtz, W.; Babel, D. *Solid State Commun.* **1983**, *48*, 277.
(13) Gadet, V.; Bujoli-Doeuff, M.; Force, L.; Verdaguer, M.; Malkhi, K. E.; Deroy, A.; Besse, J. P.; Chappert, C.; Veillet, P.; Renard, J. P.; Beauvillain, P. In *Magnetic Molecular Materials*; Gatteschi, D., Kahn, O., Miller, J. S., Palacio, F., Eds.; NATO ASI Series E; Plenum: New York, 1991; Vol. 198.
(14) Gadet, V.; Mallah, T.; Castro, I.; Verdaguer, M. *J. Am. Chem. Soc.* **1992**, *114*, 9213.
(15) Mallah, T.; Thibéaut, S.; Verdaguer, M.; Veillet, P. *Science* **1993**, *262*, 1554.
(16) Mallah, T.; Ferlay, S.; Auberger, C.; Helary, C.; L'Hermite, F.; Ouahès, R.; Vassermann, J.; Verdaguer, M.; Veillet, P. *Mol. Cryst. Liq. Cryst.* **1994**, *273*, 141.
(17) Ferlay, S.; Mallah, T.; Ouahès, R.; Veillet, P.; Verdaguer, M. *Nature* **1995**, *378*, 701.
(18) Entley, W. R.; Treadway, C. R.; Girolami, G. S. *Mol. Cryst. Liq. Cryst.* **1994**, *273*, 153.
(19) Entley, W. R.; Girolami, G. S. *Science* **1995**, *268*, 397.
(20) Entley, W. R.; Girolami, G. S. *Inorg. Chem.* **1994**, *33*, 5165.
(21) Sato, O.; Iyoda, T.; Fujishima, A.; Hashimoto, K.; *Science* **1996**, *272*, 704.
(22) Kahn, O. *Adv. Inorg. Chem.* **1995**, *43*, 179.
(23) Kahn, O. *Nature* **1995**, *378*, 667.
(24) Rossman, G. R.; Tsay, F. D.; Gray, H. B. *Inorg. Chem.* **1973**, *12*, 824.

10.1021/ic981262t CCC: $18.00
Published on Web 07/13/1999

of the magnetic anisotropy properties it was necessary to obtain single crystals suitable for magnetic anisotropy measurements. In other respects, the presence of both high-spin 3d and low-spin 4d spin carriers could also be expected to afford interesting situations concerning the nature of the 3d−4d interaction. In particular, the symmetry rules governing the nature of the magnetic interaction between two 3d ions have recently been found invalid for a 3d−4d pair.[26]

Our first findings were much beyond our expectations.[1−3] Large and well shaped single crystals were obtained. The investigation of their magnetic properties revealed not only strong magnetic anisotropies, but also rich magnetic phase diagrams with field-induced spin reorientation phenomena in the ferromagnetically ordered domain. We focused on the $[Mo(CN)_7]^{4-}/Mn^{2+}$ system. The reaction of $[Mo(CN)_7]^{4-}$ with Mn^{2+} affords two compounds. The chemical compositions are almost identical, $Mn_2(H_2O)_5Mo(CN)_7]\cdot 4H_2O$ (α phase) and $Mn_2(H_2O)_5Mo(CN)_7]\cdot 4.75H_2O$ (β phase); but the three-dimensional organizations differ significantly. A paper has been devoted to the structure and magnetic properties of the former compound.[2] $Mn_2(H_2O)_5Mo(CN)_7]\cdot 4H_2O$ (α phase) orders ferromagnetically at $T_c = 51$ K, without a hysteresis effect. Two additional magnetic phenomena have been observed. At zero field strength, another transition occurs at 43 K, which disappears when applying a field larger than 100 Oe along one of the crystallographic directions. For a critical value of the field applied along this direction, a field-induced spin reorientation is observed. This paper is devoted to the latter compound, $Mn_2(H_2O)_5Mo(CN)_7]\cdot 4.75H_2O$ (β phase). Before presenting our results, let us mention that when the reaction between $[Mo(CN)_7]^{4-}$ and Mn^{2+} is carried out in the presence of an excess of K^+ ions, another compound is obtained, of formula $K_2Mn_3(H_2O)_6[Mo(CN)_7]_2\cdot 6H_2O$. While the first two compounds have three-dimensional structures, this K^+-containing compound has a two-dimensional structure. It orders ferromagnetically at $T_c = 39$ K, and exhibits a field-induced spin reorientation in the magnetically ordered phase.[3]

Experimental Section

Synthesis. $K_4[Mo(CN)_7]\cdot 2H_2O$ was prepared as already described.[24,25,27] Well shaped and rather large ($1.5 \times 1.5 \times 1$ mm^3) single crystals of the title compound were obtained by slow diffusion in an H-shaped tube under nitrogen of two deoxygenated 10^{-4} M aqueous solutions containing $K_4[Mo(CN)_7]\cdot 2H_2O$ and $[Mn(H_2O)_6](NO_3)_2$, respectively.[23] Actually, two kinds of crystals were obtained. They were denoted as α and β phase, respectively, even if "phase" in principle should apply to compounds with strictly the same chemical composition. The crystals of the β phase to which this paper is devoted have the shape of irregular hexagonal prisms (see Figure 5) while those of the α phase have the shape of plates. The *a*, *b*, and *c** axes are also shown in Figure 5.

Crystallographic Data Collection and Structure Determination. Data were collected at room temperature on an Enraf-Nonius CAD4 diffractometer with Mo−Kα radiation. After a semiempirical Ψ-scan[28] absorption correction, the data reduction was performed using MolEN[29] while the structure of the solution and subsequent refinement were carried out using the programs SHELXS-86 and SHELXL-93.[30] The crystal data are summarized in Table 1. Diffraction studies verified that the crystal structure was retained at 25 K.

Table 1. Selected Crystal Data for $Mn_2(H_2O)_5Mo(CN)_7\cdot 4.75H_2O$

empirical formula	$C_7H_{19.5}N_7O_{9.75}Mn_2Mo$
fw	563.62
space group	$P2_1/c$
a, Å	7.885(3)
b, Å	10.406(7)
c, Å	25.233(11)
β, deg	98.11(2)
V, Å^3	2050(2)
Z	4
ρ_{calcd}, g cm^{-3}	1.826
no. of data	4917
μ (Mo Kα), cm^{-1}	0.710 73
R1[a]	0.0475
wR2[b]	0.1025

[a] $R1 = \sum||F_o| - |F_c||/\sum|F_o|$. [b] $wR2 = \{\sum[w(F_o^2 - F_c^2)^2]/\sum[w(F_o^2)^2]\}^{1/2}$.

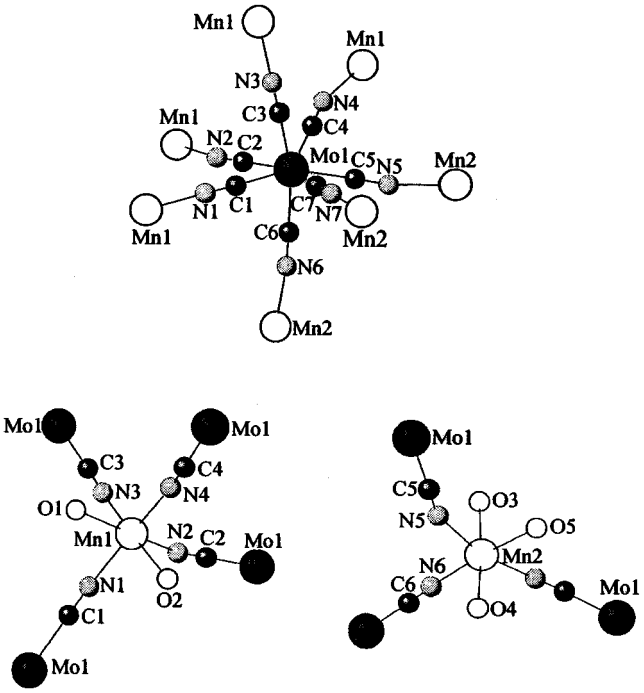

Figure 1. Local structure of the molybdenum and manganese sites.

Magnetic Measurements. These were carried out with a Quantum Design MPMS-5S SQUID magnetometer working down to 2 K and up to 50 kOe. This apparatus was equipped with a horizontal goniometer. The compound is air sensitive, and all the magnetic investigations were carried out with either single crystals embedded in an oil envelope, or polycrystalline samples placed in a quartz tube sealed under vacuum. Owing to the very large magnetic response of the compound, the diamagnetic correction, estimated at $-250\ 10^{-6}$ emu mol^{-1}, may be neglected. Similarly, the magnetic response of the oil envelopes protecting the single crystals was checked to be negligibly weak.

Description of the Structure

The structure possesses one molybdenum site along with two manganese sites, noted Mn1 and Mn2, as shown in Figure 1. The Mo atom is surrounded by seven −C−N−Mn linkages, four involving an Mn1 site and three involving an Mn2 site. The Mo−C bond lengths range from 2.110(7) to 2.191(7) Å,

(25) Hursthouse, M. B.; Maijk, K. M. A.; Soares, A. M.; Gibson, J. F.; Griffith, W. P. *Inorg. Chim. Acta* **1980**, *45*, L81.
(26) Larionova, J.; Mombelli, B.; Sanchiz, J. Kahn, O. *Inorg. Chem.* **1998**, *37*, 679.
(27) Young, R. C. *J. Am. Chem. Soc.* **1932**, *54*, 1402.
(28) North, A. C. T.; Philips, D. C.; Mathews, F. S. *Acta Crystallogr., Sect. A* **1968**, *A24*, 351.
(29) *MolEN* (Molecular Structure Enraf-Nonius); Enraf-Nonius: Delft, The Netherlands, 1990.
(30) (a) Sheldrick, G. M. *SHELXS-86: Program for the Solution of Crystal Structure*; University of Göttingen: Germany, 1986. (b) Sheldrick, G. M. *SHELXL-93: Program for the Refinement of Crystal Structure*; University of Göttingen: Germany, 1993.

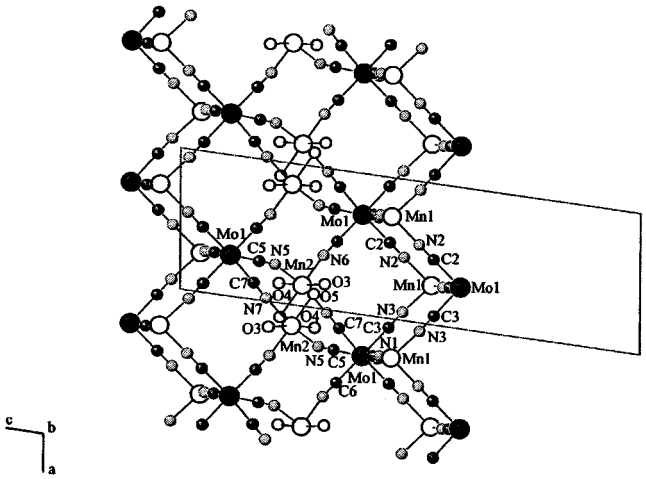

Figure 2. Structure in the *ac* plane showing two bent ladders running along the *a* direction together with the $Mn2(CN)_3(H_2O)_3$ linkages.

with a mean value of 2.147 Å. The environment around the Mo atom may be viewed as a distorted pentagonal bipyramid. Mo−C3 and Mo−C6 are the axial directions, with a C3−Mo−C6 angle of 161.0(3)°. The bond angles in the equatorial plane range from 71.8(3) to 77.9(3)°, and their sum is equal to 373.6° instead of 360° for a perfect D_{5h} geometry. All of the Mo−C−N bond angles are very close to 180°; they range from 177.1(7) to 179.8(6). On the other hand, several of the Mn−N−C bond angles deviate significantly from 180°; they range from 156.9(7) to 177.2(6)°, the mean value being 169.4°. The Mn1 site is in a distorted octahedral environment. It is surrounded by four −N−C−Mo linkages and two water molecules in a *cis* conformation. The Mn1−N bond lengths range from 2.158(5) to 2.178(6) Å, and the Mn1−O bond lengths are equal to 2.280(6) and 2.350(5) Å. The bond angles range from 81.0(2) to 102.2(3)° on one side, and from 156.5(3) to 175.1(3)° on the other side, instead of 90° and 180° for a perfect octahedron. The Mn2 site is also in a distorted octahedral environment; it is surrounded by three −N−C−Mo linkages along with three water molecules with a *mer* configuration. The Mn2−N bond lengths range from 2.175(6) to 2.190(6) Å, and the Mn2−O bond lengths range from 2.223(6) to 2.242(6) Å. The bond angles range from 82.0(3) to 98.1(3)° on one side, and from 164.5(3) to 175.5(2)° on the other side.

The three-dimensional organization may be described in two ways. The first description arises from the previously given description for the α phase.[2] We consider two kinds of centrosymmetric lozenge motifs, $[MoC2N2Mn1N4C4]_2$ and $[MoC3N3Mn1N4C4]_2$. These motifs alternate along the *a* axis by sharing the MoC4N4Mn1 edge, and form in the shape of bent ladders, or accordions. Each bent ladder of this kind is linked to two other ladders (instead of four for the α phase) along the *b* direction through cyano bridges, C1N1. The ladders are further connected by $Mn2(CN)_3(H_2O)_3$ linkages situated between the ladders. Each Mn2 site is linked though cyano bridges to two Mo atoms of a ladder and one Mo atom of an adjacent ladder, as shown in Figure 2. The Mo−Mn separations through a cyano bridge range from 5.358(2) to 5.509(4) Å.

The second description of the structure is as follows: $(MoCNMn1NC)_2$ lozenge motifs share their edges to form corrugated grids parallel to the *ab* plane, as shown in Figure 3. These grids are connected to each other along the *c* direction by $Mn2(CN)_3(H_2O)_3$ linkages. Each Mn2 site is linked though cyano bridges to two Mo atoms of one grid and one Mo atom of an adjacent grid. The structure as a whole is represented in Figure 4. This second description does not highlight the similarities and differences between the α and β phases. On the other hand, it seems to us to be easier to visualize.

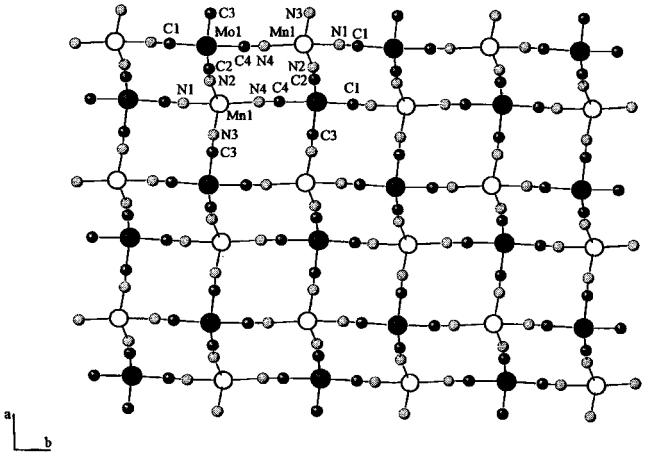

Figure 3. Structure in the *ab* plane showing a corrugated grid.

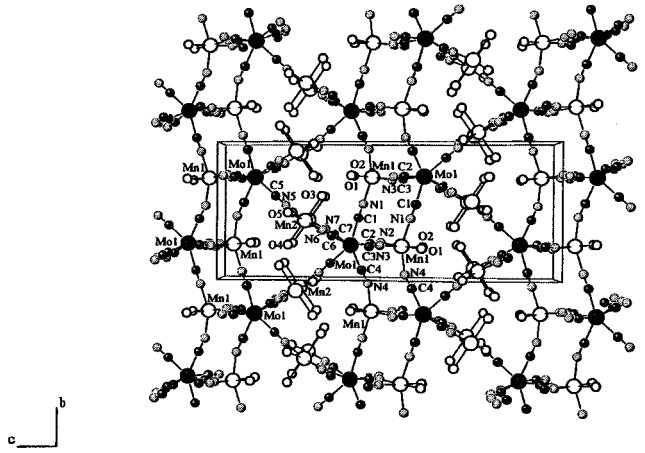

Figure 4. Structure of the compound viewed along the *a* direction.

Magnetic Properties

Determination of the Magnetic Axes. The 2-fold axis of the monoclinic lattice, *b*, is necessarily a magnetic axis.[31] To confirm that it was so, the angular dependence of the magnetization in the *ab* plane at 10 K was measured. The results are shown in Figure 5 (top). Under 2 kOe the magnetization is at a maximum along *b* and at a minimum along *a*. Increasing the external field results in a dramatic decrease of the anisotropy in the *ab* plane. This phenomenon will be discussed further below. The other two magnetic axes may be determined from the extrema of the magnetization in the *ac* plane. These extrema were found to be along the *a* and *c** directions, as shown in Figure 5 (bottom). The rotation figures of Figure 5 reveal that the *b* axis is the easy magnetization axis.

Temperature Dependence of Magnetic Susceptibility and Magnetization. Figure 6 shows the temperature dependence of $\chi_M T$ for a polycrystalline sample, in which χ_M is the molar magnetic susceptibility and T is the temperature. At room temperature, $\chi_M T$ is equal to 9.12 cm^3 K mol^{-1}, which corresponds to the expected value for two Mn^{2+} and one Mo^{3+} ion, with the local spins $S_{Mn} = {}^5/_2$ and $S_{Mo} = {}^1/_2$. As the temperature is lowered, $\chi_M T$ increases more and more rapidly,

(31) Wooster, W. A. *Tensor and Group Theory for the Physical Properties of Crystals*; Clarendon Press: Oxford, 1973.

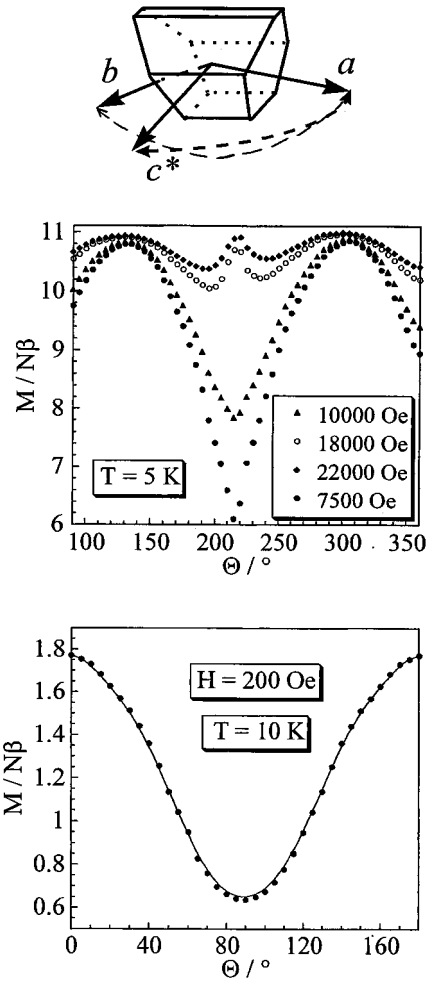

Figure 5. Angular dependence of magnetization at 10 K: (top) under different fields in the *ab* plane; (bottom) under 200 Oe in the *ac* plane.

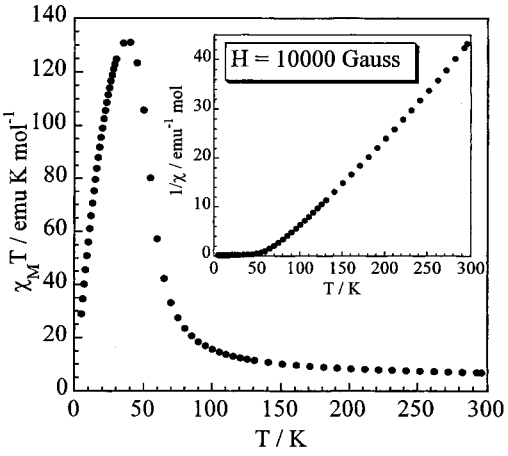

Figure 6. Temperature dependence of $\chi_M T$ for a polycrystalline sample. In the insert, temperature dependence of $1/\chi_M$.

and reaches a value of 130 cm^3 K mol^{-1} around 50 K under an applied field of 10 kOe. Such a $\chi_M T$ versus T curve is characteristic of dominant ferromagnetic interactions.[32] The $\chi_M{}^{-1}$ versus T plot displayed in the insert of Figure 6 cannot be fitted with a Curie−Weiss law.

The temperature dependence of the magnetization, M, was measured along both the *a* and *b* directions under a field of 100 Oe. The results are shown in Figure 7. The magnetization

(32) Kahn, O. *Molecular Magnetism*; VCH: New York, 1993.

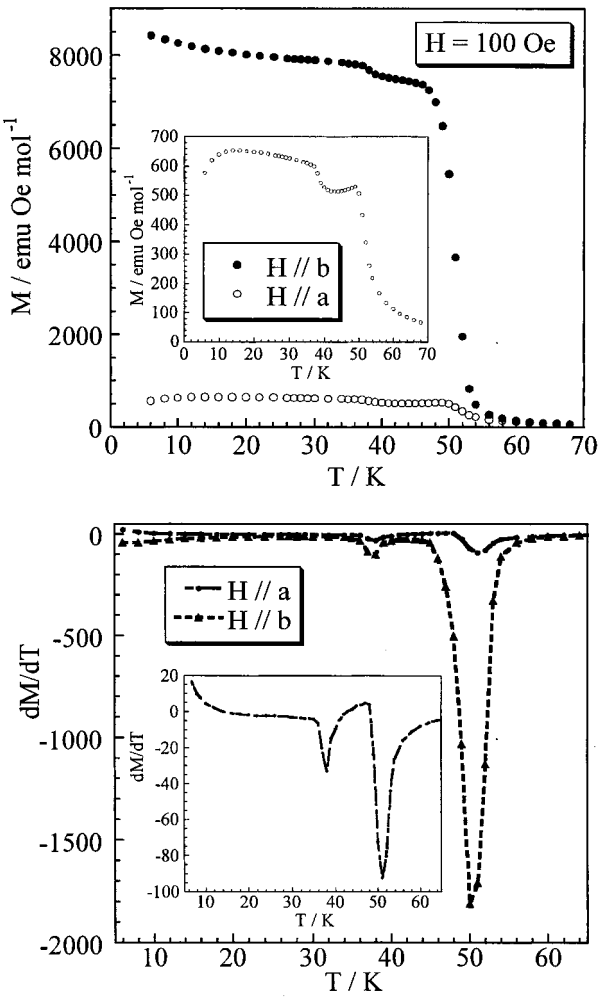

Figure 7. (top) Temperature dependence of magnetization along the *a* and *b* directions, using an external field of 100 Oe. (bottom) Temperature dependence of dM/dT.

is roughly 1 order of magnitude larger along *b* than along *a*, which confirms the strong anisotropy at low field strength. Otherwise, the two curves are qualitatively rather similar. They present four regions corresponding to the temperature ranges 2−16, 16−38, 38−51, and above 51 K. The critical temperatures under 100 Oe, $T_1 = 51$ K and $T_2 = 38$ K, were determined as the extremes of the dM/dT = $f(T)$ curves (see Figure 7, bottom).

To characterize further the magnetic transitions, the temperature dependence of the magnetization was measured along the *a* direction for different values of the field, and T_1 and T_2 were again determined as the extremes of the derivative curves, dM/dT, shown in Figure 8. As the magnetic field increases, the transition at $T_1 = 51$ K remains unchanged while the transition at lower temperature is shifted toward higher temperatures, and eventually vanishes as the field reaches 5 kOe. The temperature dependence of the fields for which the transitions are observed is shown in the insert of Figure 8.

Field Dependence of the Magnetization. The field dependence of the magnetization at 5 K along the *a*, *b*, and *c** directions is shown in Figure 9. These curves do not show any hysteresis effect. Along *b*, the zero-field susceptibility, $(dM/dH)_{H=0}$, is very high, and the saturation is reached at under 1.2 kOe. The value of the saturation magnetization, $M_S = 11\ N\beta$, corresponds exactly to what is expected for S_{Mn} and S_{Mo} spins ferromagnetically aligned along the *b* direction. Let us note that ten out of eleven unpaired electrons arise from the nearly

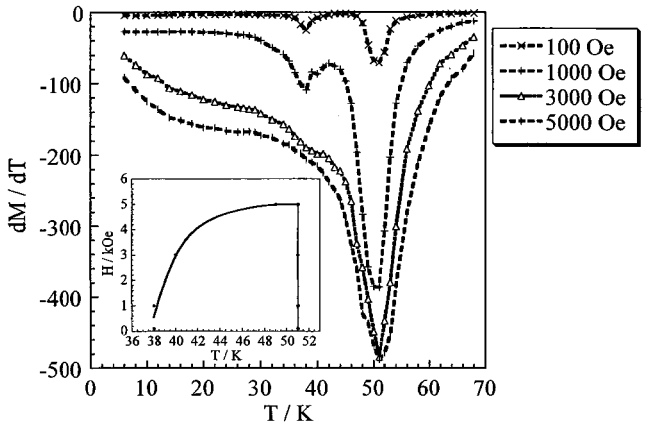

Figure 8. Temperature dependence of d*M*/d*T* along the *a* direction, using different values of the external field. In the insert, relation between critical temperatures and applied field.

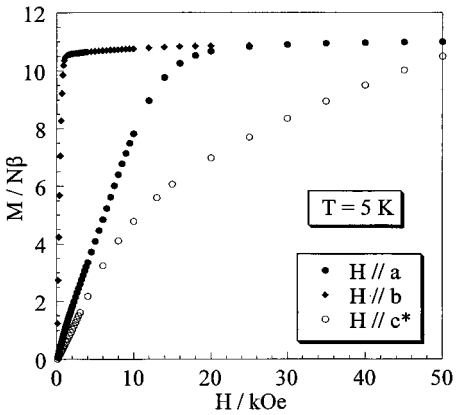

Figure 9. Field dependence of magnetization at 5 K along the *a*, *b*, and *c** directions.

isotropic Mn^{II} sites. Along *c**, the magnetization increases progressively as the field strength increases, and even at 50 kOe saturation is not reached. Along *a*, the magnetization presents an inflection point around 10 kOe, and saturation is reached at 21 kOe. This behavior characterizes a field-induced spin reorientation.[33−41] Under a low field applied along the *a* axis, the spins remain aligned along *b*. When the field reaches a critical value, H_c, the spins rotate progressively from the *b* to the *a* direction, and when the field reaches a saturation value, H_{sat}, the spins align along *a*.

It is important to mention that the curves of Figure 9 are not corrected for demagnetizing effects.[42] Such corrections are difficult to perform accurately, owing to the irregular shape of the single crystals.

(33) Stryjewski, E.; Giordano, N. *Adv. Phys.* **1977**, *26*, 487.
(34) Givord, D.; Li, H. S.; Perrier de la Bathie, R. *Solid State Commun.* **1984**, *51*, 857.
(35) Hirosawa, S.; Matsuura, Y.; Yamamoto, H.; Fujimura, S.; Sagawa, M.; Yamauchi, H. *J. Appl. Phys.* **1986**, *59*, 873.
(36) Salgueiro da Siva, M. A.; Moreira, J. M.; Mendes, J. A.; Amaral, V. S.; Sousa, J. B.; Palmer, S. B. *J. Phys.: Condens. Mater.* **1995**, *7*, 9853.
(37) Canfield, P. C.; Cho, B. K.; Dennis, K. W. *Physica B* **1995**, *215*, 337.
(38) Garcia-Landa, B.; Tomey, E.; Fruchart, D.; Gignoux, D.; Skolozdra, R. *J. Magn. Magn. Mater.* **1996**, *157−158*, 21.
(39) Mendoza, W. A.; Shaheen, S. A. *J. Appl. Phys.* **1996**, 79, 6327.
(40) Cao, G.; McCall, S.; Crow, J. E. *Phys. Rev. B* **1997**, *55*, R672.
(41) Kou, X. C.; Dahlgren, M.; Grössinger; Wiesinger, G. *J. Appl. Phys.* **1997**, *81*, 4428.
(42) Herpin, A. *Théorie du Magnétisme*; Presses Universitaires de France: Paris, France, 1968.

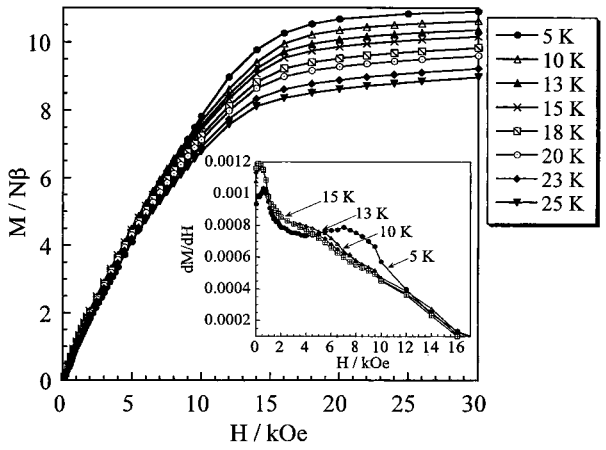

Figure 10. (top) Field dependence of magnetization along the *a* direction at different temperatures up to 25 K. In the insert, field dependence of d*M*/d*H*.

To confirm the spin reorientation along the *a* direction, the angular variation of magnetization at 5 K in the *ab* plane was measured for different field values. The results are represented in Figure 5 (top). As already mentioned, at low field strength the magnetization is minimum along *a*. As the field strength increases, the magnetization along *a* increases from the minimum. Eventually, for field strength values higher than 18 kOe, the magnetization along *a* is much the same as along *b*. The *ab* plane becomes almost isotropic.

Figure 10 shows the field dependence of magnetization along *a* at different temperatures up to 25 K. For each field, the value of the critical field was determined from the extreme of the derivative d*M*/d*H*, and the value of the saturation field as the smallest field of the linear regime of the $M = f(H)$ curve. The inflection point of the $M = f(H)$ curves disappears when the temperature reaches 16 K, which seems to indicate that the spin reorientation phenomenon is limited to the temperature range below 16 K. The temperature dependence of H_c and H_{sat} is displayed in Figure 12. These curves will be utilized in an attempt to determine the magnetic phase diagram of the compound.

Determination of the Spontaneous Magnetization. The field dependence of the magnetization along the *b* axis was measured at different temperatures in the 0−51 K temperature range. At each temperature, the spontaneous magnetization was determined by extrapolating at zero field strength the linear part of the curve at high field strength. The temperature dependence of the normalized spontaneous magnetization obtained in this way is represented in Figure 11 (bottom, circles). When working along the other two magnetic axes, *a* and *c**, a different temperature dependence of spontaneous magnetization is obtained. This situation is most likely due to the occurrence of several additional magnetic transitions below 51 K. To obtain information on all the crystallographic directions, the field dependence of magnetization was measured at different temperatures along the [111] direction corresponding to the principal diagonal of the single crystal. The results are shown in Figure 11 (top). The temperature dependence of spontaneous magnetization deduced from this study along the [111] direction is also shown in Figure 11 (bottom, triangles). It reveals three transitions, at 16, 38, and 51 K.

Magnetic Phase Diagram: First Approach

The magnetic data presented above allows us to propose the magnetic phase diagram shown in Figure 12 for a magnetic field

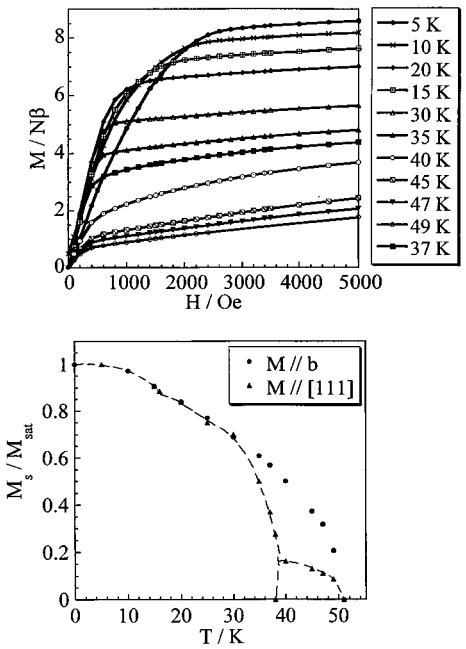

Figure 11. (top) Field dependence of magnetization along the [111] direction at different temperatures up to 51 K. (bottom) Temperature dependence of normalized spontaneous magnetization along the *b* and [111] directions (see text).

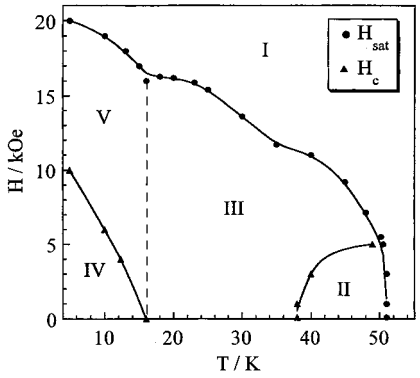

Figure 12. Tentative magnetic phase diagram; the solid lines are guidelines joining the experimental points, and the dotted line represents a boundary which has not been determined experimentally, but is postulated (see text).

applied along the *a* direction. This diagram contains five domains, noted I−V. Domain I corresponds to the paramagnetic (or saturated paramagnetic) domain in which the spins are disordered. Domains II, III, and IV are ferromagnetic domains in which the spins are perfectly (or essentially) aligned along the *b* direction. Domain V, finally, is a spin reorientation domain corresponding to the rotation of the spins from the *b* to the *a* direction as the field along *a* increases from H_c to H_{sat}. The boundaries shown in solid lines in Figure 12 were effectively determined in this study. On the other hand, the dotted line boundary between domains III and V could not be experimentally observed. This boundary was plotted for consistency.

The differences between the magnetically ordered domains II, III, and IV remain unknown. Perhaps they differ by some degrees of canting. Neutron diffraction experiments may make it possible to specify the different magnetic structures.

Discussion

The reaction of $[Mo(CN)_7]^{4-}$ with Mn^{2+} affords two compounds whose chemical formulas are very close to each other. They are *pseudo*-polymorphs. The local environments of the molybdenum and manganese sites are also very similar, but the three-dimensional organizations are rather different. In both cases, bent ladders formed by edge-sharing $(MoCNMn1NC)_2$ lozenge motifs run along the *a* axis. In the α phase, each bent ladder is surrounded by four other ladders while in the *β* phase, investigated in this paper, each bent ladder is surrounded by two other ladders. For both compounds, these ladders are further connected by $Mn2(CN)_3(H_2O)_3$ linkages.

The structural differences lead to substantial differences as far as the magnetic properties are concerned. The magnetic phase diagram for the title compound is even more complex than for the α phase. Both the α and *β* phases exhibit a three-dimensional ferromagnetic ordering at $T_c = 51$ K. For the α phase an additional transition, occurring between two magnetically ordered phases, has been observed at 43 K at zero field strength. This transition is shifted toward higher temperatures as the field is increased, and eventually vanishes under a field of 100 Oe. For the *β* phase, an additional transition between two magnetically ordered states has also been characterized. The transition temperature occurs at 38 K at zero field strength and, as is also the case for the α phase, is shifted toward higher temperatures as the field increases. However, a much higher field strength, about 5 kOe, needs to be applied to suppress this transition.

Both compounds exhibit a field-induced spin reorientation when the field is applied along the *a* axis, but again the magnetic behaviors are quantitatively different. For the α phase, the spin reorientation occurs at any temperature below $T_c = 51$ K. When the field strength along the *a* axis is lower than a critical value, varying from zero to 2.3 kOe as the temperature is lowered, the spins align along the easy magnetization axis *b*. Between the critical value and the saturation value, the spins rotate from the *b* to the *a* axis. The saturation field strength varies from zero at 51 K to 2.7 kOe at low temperatures. Finally, when the field is higher than the saturation value, the spins align along *a*. For the *β* phase, the spin reorientation seems to be limited to the temperature range below 16 K. The critical and saturation field values are then much higher. They reach 10 and 20 kOe, respectively, at very low temperatures. It follows that the mixed domain between H_c and H_{sat} (domain V in Figure 12), in which the spins rotate, is more limited in temperature and much extended in field strength range for the *β* phase.

We must emphasize again that the magnetic phase diagram for the title compound is far from fully understood. The boundary between domains IV and V has not been experimentally observed. Its existence was postulated for internal consistency. Moreover, magnetic measurements, even on single crystals, do not allow a specification of the exact differences between the magnetically ordered domains, noted II, III, and V in Figure 12. All three are ferromagnetic domains in which the spins are (essentially) aligned along the *b* axis. Probably, they differ by some degrees of canting. In other respects, the *β* phase is even more anisotropic than the α phase. For instance, the field which must be applied along the *a* axis to rotate the spins is roughly five times as large in the *β* phase as in the α phase. So far, we do not see what structural factors could justify such a difference.

Both the α and *β* phases contain some noncoordinated water molecules which can be easily released under vacuum at room temperature. We have seen that the partial dehydration of the α phase modifies dramatically the magnetic properties.[2] T_c is increased from 51 to 65 K, and in the ferromagnetic domain the compound presents a hysteresis loop with a coercive field of 0.85 kOe at 5 K. The *β* phase was also dehydrated under the

same experimental conditions. The critical temperature was then found to be the same as for the α phase after dehydration, and the coercive field at 5 K was found as 1.8 kOe. The X-ray powder patterns of the dehydrated α and *β* phases were recorded, and found to be identical. These patterns are compatible with none of the structures of hydrated crystals. The different values of the coercive field reflect the fact that the coercivity is not an intrinsic property, but depends on structural factors such as the grain size.

One of the most striking features of the three compounds obtained so far in the $[Mo(CN)_7]^{4-}-Mn^{2+}$ system is the ferromagnetic nature of the low-spin $Mo^{3+}-$high-spin Mn^{2+} interaction through the cyano bridge. This feature was extensively discussed in a preceding paper.[2] We intend to come back to this problem in a subsequent theoretical paper.

Conclusions

The field of molecule-based magnets emerged about twelve years ago when the first molecular compounds exhibiting a spontaneous magnetization below a certain critical temperature were reported.[43,44] Up to now, researchers involved in this field, including ourselves, have focused on the characterization of the critical temperatures, and on the possible existence of magnetic hysteresis loops which confer a memory effect on the system. To the best of our knowledge, very few studies have been published so far reporting thorough single crystal investigations. Only this kind of investigation can allow the determination, at least approximately, of the magnetic phase diagram. Most often, molecular synthesis leads to low symmetry chemical objects. In the field of molecular magnetism, low symmetry implies anisotropy properties. The compound described in this paper as well as the two other compounds of the same family already described are almost textbook examples pointing out the peculiar magnetic behavior arising from this anisotropy.

Acknowledgment. This work was partly funded by the TMR Research Network ERBFMRXCT980181 of the European Union, entitled "Molecular Magnetism; from Materials toward Devices."

Supporting Information Available: A listing of crystal data and structure refinement, atomic coordinates, bond lengths and angles, anisotropic displacement parameters. This material is available free of charge via the Internet at http://pubs.acs.org.

IC981262T

(43) Miller, J. S.; Calabrese, J. C.; Rommelman, H.; Chittipedi, S. R.; Zang, W. M.; Reiff, A. J.; Epstein, J. *J. Am. Chem. Soc.* **1987**, *109*, 9, 769.

(44) Pei, Y.; Verdaguer, M.; Kahn, O.; Sletten, J.; Renard, J. P. *J. Am. Chem. Soc.* **1988**, *110*, 782.